SUPPORTING INFORMATION

DOUBLE-WELL ULTRACOLD-FERMIONS COMPUTATIONAL MICROSCOPY: WAVE-FUNCTION ANATOMY OF ATTRACTIVE-PAIRING AND WIGNER-MOLECULE ENTANGLEMENT AND NATURAL ORBITALS

Benedikt B. Brandt, Constantine Yannouleas and Uzi Landman*
School of Physics, Georgia Institute of Technology, Atlanta, Georgia 30332-0430, USA

*Corresponding Author: uzi.landman@physics.gatech.edu

1. Two-center-oscillator confining potential. Following the recent experimental advances[1-3], and in particular those in ref. 2, we investigate here the quantum mechanical properties of two interacting fermionic ultracold atoms confined in a double well (DW). We consider two DW configurations: (1) a so-called "linear arrangement" (LA) where two quasi one-dimensional (1D) wells (see below Eq. S1), connected by a barrier between them, are located on the same axis (x), and (2) a so-called " parallel arrangement" (PA) where the quasi 1D wells are oriented along two parallel lines in the y direction being separated by a barrier in the x-direction; tunneling between the wells occurs in the x-direction through the long sides of the wells (namely the sides that are along the y- axis). Case (1), the LA configuration, is described in detail in the main text of the article, and case (2), the PA configuration, is discussed (see caption to Fig. S1 below) and compared (along with the LA configuration) with the experimental results[2], see Fig. S2 below.

To model the two interacting fermionic ultracold atoms confined in a double well we use a 2D many-body problem (as described below). In the LA configuration we enforce the 1D character by requiring that the trap confinement in the y-direction is much stronger than that in the x-direction (i.e. $\omega_y / \omega_x >> 1$), with the result that only the zero-point motion in the y-direction is included in the calculations, whereas in the PA configuration we choose $\omega_y / \omega_x < 1$ (see the caption of Fig. S1 below).

In the 2D two-center-oscillator (TCO), the single-particle levels associated with the confining potential are determined by the single-particle hamiltonian[4,5]

$$H = \frac{\boldsymbol{p}^2}{2m} + \frac{1}{2}m\omega_y^2 y^2 + \frac{1}{2}m\omega_{xk}^2 x_k'^2 + V_{neck}(x) + h_k, \tag{S1}$$

where $x_k' = x - x_k$ with $k = 1$ for $x < 0$ (left well) and $k = 2$ for $x > 0$ (right well), and the h_k's control the relative well-depth, with the tilt being $\Delta = h_2 - h_1$. y denotes the coordinate perpendicular to the inter-dot axis (x). The most general shapes described by H are two semiellipses connected by a smooth neck [$V_{neck}(x)$]; $x_1 < 0$ and $x_2 > 0$ are the centers of these semiellipses, $d = x_2 - x_1$ is the interdot distance, and m is the atom mass.

For the smooth neck between the two wells, we use $V_{neck}(x) = \frac{1}{2}m\omega_{xk}^2[C_k x_k'^3 + D_k x_k'^4]\theta(|x| - |x_k|)$, where $\theta(u) = 0$ for $u > 0$ and $\theta(u) = 1$ for $u < 0$. The four constants C_k and D_k can be expressed via two parameters, as follows: $C_k = (2 - 4\epsilon_k^b)/x_k$ and $D_k = (1 - 3\epsilon_k^b)/x_k^2$, where the barrier-control parameters $\epsilon_k^b = (V_b - h_k)/V_{0k}$ are related to the actual height of the bare interdot barrier (V_b) between the two wells, and $V_{0k} = m\omega_{xk}^2 x_k^2/2$ (for $h_1 = h_2, V_{01} = V_{02} = V_0$).

The single-particle levels of H are obtained by numerical diagonalization in a (variable-with-separation) basis consisting of the eigenstates of the auxiliary hamiltonian:

$$H_0 = \frac{\boldsymbol{p}^2}{2m} + \frac{1}{2}m\omega_y^2 y^2 + \frac{1}{2}m\omega_{xk}^2 x_k'^2 + h_k\,. \tag{S2}$$

The eigenvalue problem associated with the auxiliary hamiltonian (Eq. S2) is separable in x and y, i.e., the wave functions are written as

$$\varphi_i(x, y) = X_\mu(x)Y_n(y), \tag{S3}$$

with $i \equiv \{\mu, n\}$, $i = 1,2, \ldots, K$. The $Y_n(y)$ are the eigenfunctions of a 1D oscillator, and the $X_\mu(x \le 0)$ or $X_\mu(x > 0)$ can be expressed through the parabolic cylinder functions $U[\gamma_k, (-1)^k \xi_k]$, where $\xi_k = x_k'\sqrt{2m^*\omega_{xk}/\hbar}$, $\gamma_k = (-E_x + h_k)/(\hbar\omega_{xk})$, and $E_x = (\mu + 0.5)\hbar\omega_{x1} + h_1$ denotes the x-eigenvalues. The matching conditions at $x = 0$ for the left and right domains yield the x-eigenvalues and the eigenfunctions $X_\mu(x)$. The n indices are integer. The number of μ indices is finite; however, they are in general real numbers.

2. The configuration-interaction method. As aforementioned, we use the method of configuration Interaction for determining the solution of the many-body problem specified by the

Hamiltonian (Eq. S1).

In the CI method, one writes the many-body wave function $\Phi_N^{\mathrm{CI}}(\boldsymbol{r}_1, \boldsymbol{r}_2, \ldots, \boldsymbol{r}_N)$ as a linear superposition of Slater determinants $\Psi^N(\boldsymbol{r}_1, \boldsymbol{r}_2, \ldots, \boldsymbol{r}_N)$ that span the many-body Hilbert space and are constructed out of the single-particle *spin-orbitals*

$$\chi_j(x, y) = \varphi_j(x, y)\alpha, \quad \text{if} \quad 1 \leq j \leq K, \tag{S4}$$

and

$$\chi_j(x, y) = \varphi_{j-K}(x, y)\beta, \quad \text{if} \quad K < j \leq 2K, \tag{S5}$$

where $\alpha(\beta)$ denote up (down) spins. Namely

$$\Phi_{N,q}^{\mathrm{CI}}(\boldsymbol{r}_1, \ldots, \boldsymbol{r}_N) = \sum_I C_I^q \, \Psi_I^N(\boldsymbol{r}_1, \ldots, \boldsymbol{r}_N), \tag{S6}$$

where

$$\Psi_I^N = \frac{1}{\sqrt{N!}} \begin{vmatrix} \chi_{j_1}(\boldsymbol{r}_1) & \cdots & \chi_{j_N}(\boldsymbol{r}_1) \\ \vdots & \ddots & \vdots \\ \chi_{j_1}(\boldsymbol{r}_N) & \cdots & \chi_{j_N}(\boldsymbol{r}_N) \end{vmatrix}, \tag{S(7)}$$

and the master index I counts the number of arrangements $\{j_1, j_2, \ldots, j_N\}$ under the restriction that $1 \leq j_1 < j_2 < \cdots < j_N \leq 2K$. Of course, $q = 1,2,...$ counts the excitation spectrum, with $q = 1$ corresponding to the ground state. In our CI calculations full convergence is reached through the use of a basis of up to70 TCO single-particle states; the TCO single-particle states automatically adjust to the separation d as it varies from the limit of the unified atom $d = 0$ to that of the dissociation of the dimer (for sufficiently large d).

The many-body Schrödinger equation $H\Phi_{N,q}^{\mathrm{EXD}} = E_{N,q}^{\mathrm{EXD}}\Phi_{N,q}^{\mathrm{EXD}}$ transforms into a matrix diagonalizatiom problem, which yields the coefficients C_I^q and the eigenenergies $E_{N,q}^{\mathrm{CI}}$. Because the resulting matrix is sparse, we implement its numerical diagonalization employing the well known ARPACK solver[6].

The matrix elements $< \Psi_N^I | H | \Psi_N^J >$ between the basis determinants [see Eq. (S7)] are calculated using the Slater rules[7]. Naturally, an important ingredient in this respect are the two-body matrix elements of the contact interaction,

$$g_{2\mathrm{D}} \int_{-\infty}^{\infty} \int_{-\infty}^{\infty} d\,\boldsymbol{r}_1 d\boldsymbol{r}_2 \varphi_i^*(\boldsymbol{r}_1)\varphi_j^*(\boldsymbol{r}_2)\delta(\boldsymbol{r}_1 - \boldsymbol{r}_2)\varphi_k(\boldsymbol{r}_1)\varphi_l(\boldsymbol{r}_2), \tag{S8}$$

in the basis formed out of the single-particle spatial orbitals $\varphi_i(\boldsymbol{r})$, $i = 1,2,\ldots,K$ [Eq. (S7)].
In our approach, these matrix elements are determined numerically and stored separately. The

corresponding 1D interparticle interaction strengths, g, are extracted from g_{2D} as follows

$$g = g_{2\mathrm{D}} \int_{-\infty}^{\infty} d\,u[W(u)]^4, \tag{S9}$$

where u is a dummy variable and W is the lowest-in-energy single-particle state in the y (x) direction for the LA (PA) configurations, respectively. In the LA configuration, W coincides with Y_0, whereas in the PA configuration W is a linear superposition of X_μ's due to the effect of the smooth neck.

The Slater determinants Ψ_I^N [see Eq. (S7)] conserve the third projection S_z, but not the square $\widehat{\boldsymbol{S}}^2$ of the total spin. However, because $\widehat{\boldsymbol{S}}^2$ commutes with the many-body Hamiltonian, the CI solutions are automatically eigenstates of $\widehat{\boldsymbol{S}}^2$ with eigenvalues $S(S+1)$. After the diagonalization, these eigenvalues are determined by applying $\widehat{\boldsymbol{S}}^2$ onto $\Phi_{N,q}^{\mathrm{CI}}$ and using the relation

$$\widehat{\boldsymbol{S}}^2\Psi_I^N = \left[(N_\alpha - N_\beta)^2/4 + N/2 + \sum_{i<j} \varpi_{ij}\right]\Psi_I^N, \tag{S9}$$

where the operator ϖ_{ij} interchanges the spins of fermions i and j provided that their spins are different; N_α and N_β denote the number of spin-up and spin-down fermions, respectively.

When $h_1 = h_2$ ($\Delta = 0$), the xy-parity operator associated with reflections about the origin of the axes is defined as

$$\hat{P}_{xy}\Phi_{N,q}^{\mathrm{CI}}(\boldsymbol{r}_1, \boldsymbol{r}_2, \ldots, \boldsymbol{r}_N) = \Phi_{N,q}^{\mathrm{CI}}(-\boldsymbol{r}_1, -\boldsymbol{r}_2, \ldots, -\boldsymbol{r}_N) \tag{S10}$$

and has eigenvalues ± 1. With the two-center oscillator *Cartesian* basis that we use [see Eq. S7)], it is easy to calculate the parity eigenvalues for the Slater determinants, Eq. (S7), that span the many-body Hilbert space. Because $X_\mu(x)$ and $Y_n(y)$ conserve the partial $\hat{P}_x$ and $\hat{P}_y$ parities, respectively, one finds:

$$\hat{P}_{xy}\Psi_I^N = (-)^{\sum_{i=1}^N (m_i+n_i)}\Psi_I^N, \tag{S11}$$

where m_i and n_i count the number of single-particle states associated with the bare two-center oscillator [see the auxiliary Hamiltonian H_0 in Eq. (S2)] along the x axis and the simple

oscillator along the y direction (with the assumption that the lowest states have $m = 0$ and $n = 0$, since they are even states). We note again that the index μ in Eq. S3 is not an integer in general, while m here is indeed an integer (since it counts the number of single-particle states along the x direction).

3. Results for the double well parallel arrangement (PA) configuration.

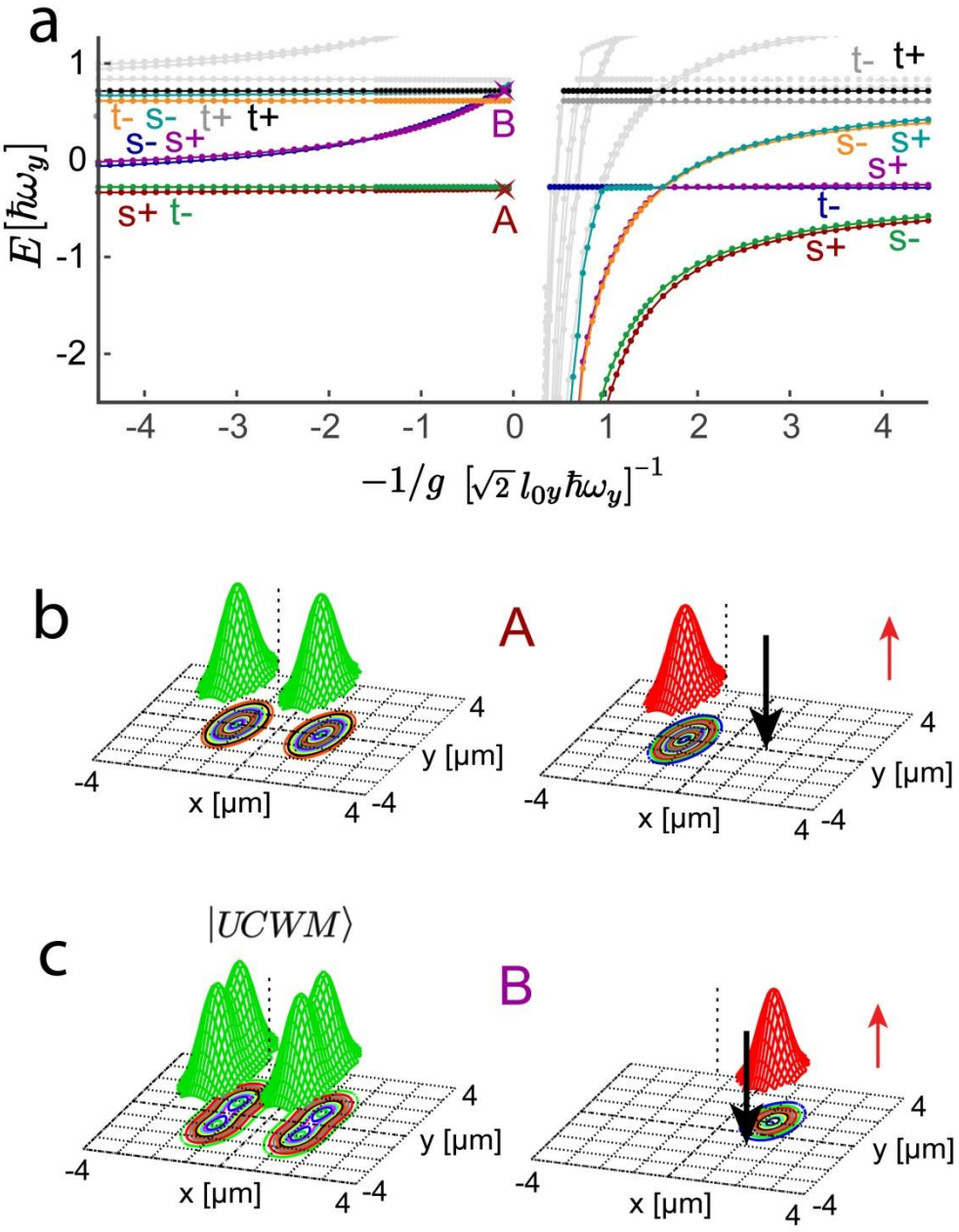

Figure S1

Figure S1. The energy spectrum (a) of two fermions and wave-function anatomy (b,c) calculated in a double well for the PA configuration. The results are plotted for a configuration with a well separation along the x-axis $d = 2.5\ \mu\text{m} = 3.51\, l_0$ ($l_0 \equiv l_{0x} = \sqrt{\hbar/(M\omega_x)}$ = 713 nm) and no tilt ($\Delta = 0$), plotted as a function of the inverse interaction strength $-1/g$; g is expressed in units of $\sqrt{2}l_{0y}\hbar\omega_y$, where $l_{0y} = \sqrt{\hbar/(M\omega_y)}$ = 1297 nm. The confining frequencies in the x and y directions are $\omega_x = 2\pi \times 6.6$ kHz and $\omega_y = 2\pi \times 1$ kHz. The barrier heights V_b (produced by the smooth neck) are given by $V_b/h = 0.49\, V_0/h = 10kHz$, where V_0 is the bare barrier of the TCO double well; V_0/h = 20.4 kHz. The mass corresponds to ultracold ^{6}Li atoms, $M = 9.99\ 10^{-27}$ kg. The DW parameters are within the range of those used in the experiments[2].

(a) Both repulsive ($\boldsymbol{-1/g < 0}$) and attractive ($\boldsymbol{-1/g > 0}$) interparticle interactions are considered. The horizontal curves correspond to Heitler-London (HL)-type states (one fermion in each well) that relate to the maximally spin-entangled two-qubit Bell states. Due to parity conservation, the $\boldsymbol{g}$-dependent, doubly-degenerate first-excited (dark blue and violet) energy curves in the repulsive regime correspond to highly space-entangled NOON-type states of the form $(|\mathbf{2,0}> \pm |\mathbf{0,2}>)/\sqrt{\mathbf{2}}$. **(b** and **c)** The many-body wave-function anatomy (single-particle densities, SPD green surfaces, and spin-resolved conditional probability distributions, CPDs, red surfaces) is illustrated for two instances, marked by letters A (shown in (b)) and B (shown in (c)) on the energy curves (in a). The abscissa value associated with these letters is $\boldsymbol{-1/g = -0.1/(\sqrt{2}l_{0y}\,\hbar\omega_y)}$. The far-left part of the $\boldsymbol{-1/g}$ axis represents the non-interacting limit. Point A (on the s+, positive parity singlet, brown line) is a representative of the above-mentioned HL-type state, and point B (on the s+ , positive parity singlet, purple line) is a representative of a NOON state. In the spin-resolved CPDs (red surfaces) the black down arrow represents the location of the spin-down fermion (taken at one of the humps in the single-particle density plots (green surfaces)), and the red arrow signifies that the red surface corresponds to the up-spin probability distribution. In (b) placing the down-spin fermion at the position of the right well (black down arrow in the position of the right density hump) shows that the distribution of the up-spin fermion (red surface) is found to be located in the other (left) well. The SPD and CPD depicted in (c) are of particular interest, representing a NOON state formed by the superposition of two-fermion ultracold Wigner molecules (UCWMs) located in either the right or left wells.

The double-humped SPDs indicate that the two fermions (due to the large repulsion) localize and avoid each other, forming an UCWM. The displayed CPD in (c) confirms formation of a UCWM – indeed, placing the down-spin fermion (black down arrow) at the position of the forward density hump in the right well, the distribution of the up-spin fermion (red surface) is found to be located away from the black arrow with its maximum coinciding with the backward hump in the SPD in the right well. If the fixed (observation) point is chosen to be in the left well, the resulting CPD will be a mirror image of the one shown above, namely it will depict a red surface in the left well. Note that the formation of NOON states is due to the conservation of parity when the detuning tilt (Δ) between the wells vanishes (as is the case here).

4. Comparison with experiment. To compare with the experimental results[2] regarding single and double occupancy as a function of the interaction strength, g, we first extract from our calculations the relevant Hubbard-model parameters. For the purpose of this comparison we use our calculations for the DW systems in the linear arrangement, LA, and parallel arrangement, PA. For the LA case we use the following parameters (see caption to Fig. 1c in the main text): The confining frequencies in the $\boldsymbol{x}$ and $\boldsymbol{y}$ directions are $\omega_x = 2\pi \times 1$ kHz and $\omega_y = 2\pi \times 100$ kHz, leading to an effective 1D confinement along the $\boldsymbol{x}$ direction. The barrier height V_b (produced by the smooth neck) is $V_b/h = 18.18\, V_0/h$ = 5.407 kHz, where V_0 is the bare barrier of the TCO double well , V_0/h = 0.297 kHz, where h is the Planck constant.. This factor leads to strong anharmonicities in the confining double-trap potential. The interwell separation is $d = 2\ \mu m = 1.543 l_0$, representing two rather well-separated wells, with $l_0 \equiv l_{0x} = \sqrt{\hbar/(M\omega_x)}$ = 1.297 μm being the (left or right) harmonic-oscillator length. The mass corresponds to ultracold ^{6}Li atoms, $M = 9.99\ 10^{-27}$ kg. For the PA case we use the parameters given in the caption to Fig. S1. These parameters correspond to those used in the experiment[2], selected there in order to assure applicability of the Hubbard model employed in reference 2, due to the small tunneling (hopping parameter J) between the two wells. .

The Hubbard-model hopping parameter is obtained from the energy spectrum of the non-interacting case for the symmetric double well (with $\Delta = 0$), i.e., the energy difference, 2J, between the singlet ground state and the first-excited triplet state . In this way we extracted for the LA configuration a value of $J/h = 48.73$ Hz, and for the PA configuration J/h = 55.53 Hz, which are sufficiently small compared to the axial trap frequency 1 kHz for the LA and PA

configurations, corresponding to the weak tunneling regime as in the experiments.

The Hubbard parameter U (the onsite interparticle interaction strength) as a function of g (where g is the contact interaction strength in the microscopic hamiltonian given in Eq. 1 of the main text) is the energy difference, $\mathrm{E}(-1/g) - \mathrm{E}(-\infty)$, for the singlet ground state in a single well; $\mathrm{E}(-\infty)$, is the energy of two non-interacting particle in a single well. If the calculations of U were to be done for the symmetric ($\Delta = 0$) case, the results would contain contributions from interwell tunneling. To minimize interwell tunneling we performed (for both the LA and PA configurations) the above evaluation for U in a strongly tilted DW configuration, so that the low energy spectrum is determined solely by the lower lying well. This also incorporates the effect of anharmonicity which is inherent to the DW confinement; this effect is particularly important in the LA configuration. In these calculations we use a tilt of $\Delta/\mathrm{h} = 4.84$ kHz for the LA configuration and $\Delta/\mathrm{h} = 9.67$ kHz for the PA configuration, while keeping the other trap parameters unchanged.

Having established the $U(g)$ dependence, we carry out a series of CPD calculations for the *symmetric* double well (with the same d and V_b) where the fixed point is placed in the left well ($x < 0$). The portion of the CPD for $x < 0$ yields the probability of double occupancy. On the other hand, the portion of the CPD for $x > 0$ yields the single-occupation probability.

Our calculations compared to the experimental measurements are displayed in Fig. S2.

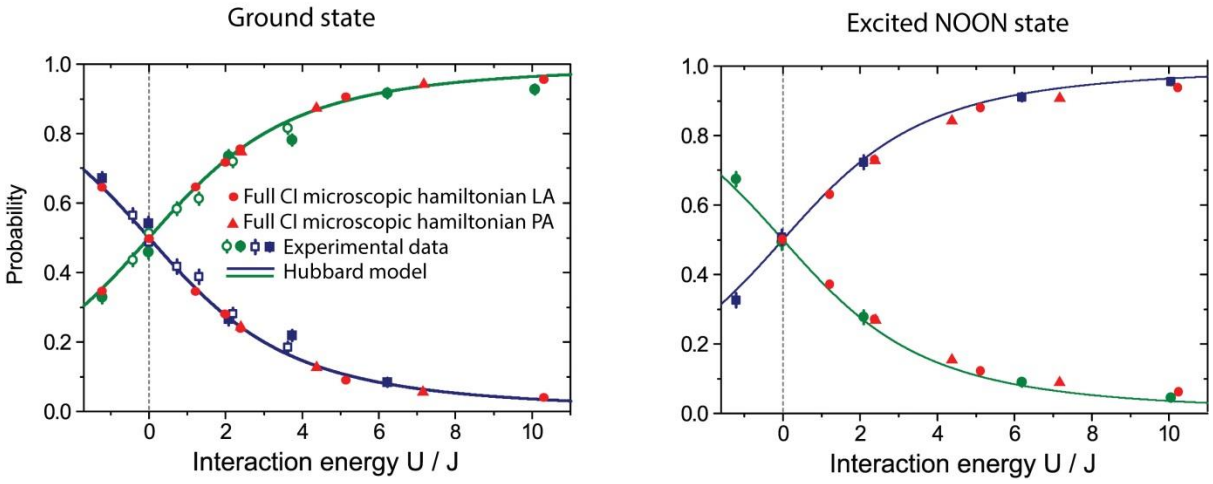

Figure S2

Figure S2. **Probability of double (blue curve) and single (green curve) occupations of the**

left and right wells for the LA and PA double well configurations. For the ground state probabilities (left frame) of both configurations we use the s+ singlet ground state (brown curve in Fig. 1c in the main text and in Fig. S1, for the LA and PA, respectively). For the excited NOON state (right frame) we use in the LA configuration the orange s+ singlet of Fig 1c (main text), and in the PA configuration we use the purple s+ singlet curve of Fig. S1. For both DW arrangements we carried out calculations for two repelling ^{6}Li atoms in a symmetric ($\Delta = 0$) double well, with the parameters of the calculations described for the LA configuration in the main text (see captions to Fig. 1) and the start of this subsection, and for the PA configuration the parameters are given in the caption of Fig. S1. Blue squares and green circles represent experimental data from Ref. 2. Red circular dots represent our CI simulation results for the LA configuration, and red triangles correspond to our calculated results for the PA configuration. Note the interchange between the blue and green probability curves (compared to the left panel), which is found both in theory and the experiment. Note that the calculated results for both the LA and PA configurations of the double well system agree well with the experimentally measured data. The limit of the Hubbard model cannot distinguish between the two microscopic trap arrangements.

References

(1) Serwane, F.; Zürn, G.; Lompe, T.; Ottenstein, T.B.; Wenz, A.N; Jochim, S. *Science* **2011**, *332*, 336-338.

(2) Murmann, S.; Bergschneider, A.; Klinkhamer, V.M.; Zürn, G.; Lompe, Th.; Jochim, S. *Phys. Rev. Lett.* **2015**, *114*, 080402.

(3) Kaufman, A.M.; Lester, B.J.; Reynolds, C.M.; Wall, M.L.; Foss-Feig, M.; Hazzard, K.R.A.; Rey, A.M.; Regal, C.A. *Science* **2014**, *345*, 306-309.

(4) Li, Y.; Yannouleas, C.; Landman, U. *Phys. Rev. B* **2009**, *80*, 045326.

(5) Yannouleas, C.; Landman, U. *Int. J. Quantum Chem.* , **2002**, *90*, 699-708.

(6) Lehoucq, R.B.; Sorensen, D.C.; Yang, C. *ARPACK Users' Guide: Solution of Large-Scale Eigenvalue Problems with Implicitly Restarted Arnoldi Methods*, SIAM, Philadelphia, **1998**.

(7) Szabo, A.; Ostlund, N.S. *Modern Quantum Chemistry*, McGraw-Hill, New York, **1989**.